HHS Public Access

Author manuscript

Cell Rep. Author manuscript; available in PMC 2021 September 08.

Published in final edited form as:

Cell Rep. 2021 August 10; 36(6): 109506. doi:10.1016/j.celrep.2021.109506.

Feedback repression of PPARα signaling by *Let-7* microRNA

Tomoki Yagai[1,5,6], **Tingting Yan**[1,5], **Yuhong Luo**[1,5], **Shogo Takahashi**[1,2], **Daisuke Aibara**[1,3], **Donghwan Kim**[1], **Chad N. Brocker**[1], **Moshe Levi**[2], **Hozumi Motohashi**[4], **Frank J. Gonzalez**[1,7,*]

[1]Laboratory of Metabolism, Center for Cancer Research, National Cancer Institute, National Institutes of Health, Bethesda, MD 20892, USA

[2]Department of Biochemistry and Molecular and Cellular Biology, Georgetown University, Washington DC, USA

[3]Faculty of Pharmaceutical Science, Fukuoka University, 8-19-1 Nanakuma, Jonan-ku, Fukuoka 814-0180, Japan

[4]Department of Gene Expression Regulation, Institute of Development, Aging and Cancer, Tohoku University, Sendai 980-8575, Japan

[5]These authors contributed equally

[6]Present address: Department of Metabolic Bioregulation, Institute of Development, Aging and Cancer, Tohoku University, Sendai 980-8575, Japan

[7]Lead contact

SUMMARY

Peroxisome proliferator-activated receptor α (PPARα) controls hepatic lipid homeostasis and is the target of lipid-lowering fibrate drugs. PPARα activation represses expression of *let-7* microRNA (miRNA), but the function of *let-7* in PPARα signaling and lipid metabolism is unknown. In the current study, a hepatocyte-specific *let-7b/c2* knockout (*let7b/c2*$^{\Delta Hep}$) mouse line is generated, and these mice are found to exhibit pronounced resistance to diet-induced obesity and fatty liver. *Let-7* inhibition by hepatocyte-specific let-7 sponge expression shows similar phenotypes as *let7b/c2*$^{\Delta Hep}$ mice. RNA sequencing (RNA-seq) analysis reveals that hepatic PPARα signaling is repressed in *let7b/c2*$^{\Delta Hep}$ mice. Protein expression of the obligate PPARα heterodimer partner retinoid X receptor α (RXRα) is reduced in the livers of *let7b/c2*$^{\Delta Hep}$ mice. Ring finger protein 8 (*Rnf8*), which is a direct target of *let*-7, is elevated in *let7b/c2*$^{\Delta Hep}$ mouse liver and identified as a E3 ubiquitin ligase for RXRα. This study highlights a let-7-RNF8-RXRα regulatory axis that modulates hepatic lipid catabolism.

*Correspondence: gonzalef@mail.nih.gov.

AUTHOR CONTRIBUTIONS

T. Yagai, T. Yan, Y.L., S.T., D.A., D.K., and C.N.B. performed the research and analyzed the data. T. Yagai, T. Yan, M.L., H.M., and F.J.G. designed and supervised the research and wrote the manuscript.

DECLARATION OF INTERESTS

The authors declare no competing interests.

SUPPLEMENTAL INFORMATION

Supplemental information can be found online at https://doi.org/10.1016/j.celrep.2021.109506.

In brief

Yagai et al. identify a negative feedback loop involving PPARα/RXRα control of hepatic lipid metabolism. The study demonstrates let-7 microRNA repression by PPARα activation, RNF8 mRNA and protein decay by let-7 microRNA, and RXRα protein degradation by RNF8 E3 ubiquitin ligase.

Graphical Abstract

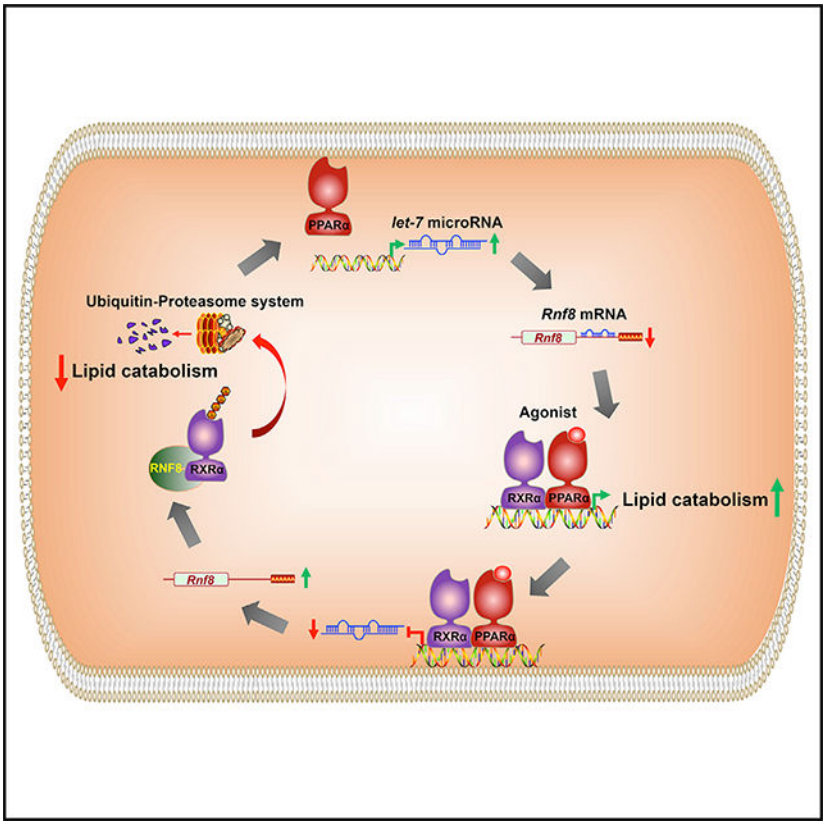

INTRODUCTION

Let-7 microRNA (miRNA), which is one of the first miRNAs discovered, plays significant roles in embryogenesis, development, metabolism, and oncogenesis (Büssing et al., 2008; Jovanovic and Hengartner, 2006; Schickel et al., 2008; Stefani and Slack, 2008). *Let-7c* belongs to the *let-7* family, with the mature sequence being highly similar among the family members and sharing the same target messenger RNAs (mRNAs). A previous study revealed that mature *let-7c* and its primary transcript, long non-coding RNA (lncRNA) *AK033222* (also known as *Mir99ahg*), were potently and rapidly repressed by activation of hepatic peroxisome proliferator-activated receptor α (PPARα), a nuclear receptor that predominantly modulates lipid metabolism (Shah et al., 2007). *Let-7* miRNA potentiates the decay of mRNAs and inhibits protein translation related to cell proliferation, cell differentiation, immune response, and glucose metabolism (Johnson et al., 2005; Liu et al., 2011; Mayr et al., 2007; Schulte et al., 2011; Zhu et al., 2011). Whole-body *let-7* inhibition

in transgenic mice expressing *Lin28a* or *Lin28b* results in resistance to hepatic steatosis and obesity (Zhu et al., 2011), and glucose metabolism is also partially improved by a global *let-7* inhibitor (Frost and Olson, 2011), suggesting a role for *let-7* in modulating glycolipid metabolism. However, how hepatic *let-7* modulates lipid metabolism remains unknown.

In this study, PPARα activation by synthetic Wy-14,643 or endogenous ligands was found to suppress expression of the *let-7* family, an effect dependent on hepatic PPARα. The biological effects of hepatic *let-7* on hepatic lipid metabolism were further analyzed by use of both hepatocyte-specific *let-7b/c2* knockout (*let7b/c2*$^{\Delta Hep}$) mice and hepatocyte-specific let-7 sponge-mediated *let-7* inhibition. Hepatic *let-7* deficiency prevented hepatic steatosis and obesity induced by high-fat diet (HFD) feeding accompanied by inhibition of the PPARα signaling. Further analyses revealed that RXRα protein levels were decreased in *let-7*-disrupted hepatocytes. Ring finger protein 8 (*Rnf8*) was identified as a E3 ubiquitin ligase for RXRα, and *Rnf8* mRNA was revealed as a direct target of *let-7*. These data demonstrate that hepatic *let*-7 deficiency improves hepatic steatosis during obesity by the RNF8-RXRα axis, suggesting a let-7-RNF8-RXRα axis that may act as a negative feedback loop to attenuate PPARα-mediated lipid-modulating signaling.

RESULTS

Expression of *let-7* miRNA in response to PPARα activation

The *Let-7* miRNA family consists of 9 mature miRNAs processed from 12 precursors and 8 primary transcripts (Table S1). Although the mature *let-7–5p* sequence is highly similar among other *let-7* family members, the precursors have unique sequences in their terminal loop and 3p region. To determine the effects of PPARα activation on individual *let-7* miRNAs, the hepatic levels of the *let-7* miRNA precursors were measured in wild-type (*Ppara*$^{+/+}$) and hepatocyte-specific *Ppara* knockout (*Ppara*$^{\Delta Hep}$) mice. Wy-14,643 as a PPARα-specific agonist was used to induce hepatic PPARα activation. In response to Wy-14,643 administration, *pre-let-7a-1*, *a-2*, *b*, *c-1*, *c-2*, *e*, *f-1*, *f-2*, *g*, and *miR-98* were significantly decreased, whereas *pre-let-7d* and *pre-let-7i* tended to decrease without significance in wild-type mice but not in *Ppara*$^{\Delta Hep}$ mice (Figure 1A). The total pooled *let-7* precursor abundance was decreased by half after Wy-14643 treatment in livers of *Ppara*$^{+/+}$ mice but not *Ppara*$^{\Delta Hep}$ mice (Figure 1B). To analyze the effect of PPARα activation by endogenous ligands, mice were fasted for 24 h, which leads to increased PPARα signaling resulting from increased endogenous metabolites that are PPARα agonists (Kersten et al., 1999). Hepatic *pre-let-7a-1*, *b*, *d*, *f-1*, and *f-2* were significantly decreased in fasted wild-type mice but not in *Ppara*$^{\Delta Hep}$ mice (Figure 1C), a phenotype not observed in fed mice. The total pooled *let-7* precursor abundance was decreased by approximately 40% after fasting (Figure 1D). These data demonstrate that PPARα activation by either a chemical agonist or endogenous fatty acid induces a decrease of *let-7* expression in a hepatocyte PPARα-dependent manner.

A time course analysis of hepatic mature *let-7* expression after PPARα activation further revealed that mature *let-7* family's transcripts started to decrease by 12 h after Wy-14,643 administration. All *let-7* family members were significantly repressed within 24 h (Figure 1E). Previous studies revealed that RNA-binding proteins *Lin28a* and *Lin28b* were highly

expressed during embryogenesis and upregulated in some cancers to selectively block the maturation of *let-7*. Lin28 selectively binds the terminal loop region of let-7 precursors and inhibits miRNA processing (Piskounova et al., 2008). To explore whether Lin28 plays a role in the regulation of *let*-7 during PPARα activation, hepatic *Lin28a* and *Lin28b* were quantified in response to Wy-14643 treatment. However, Lin28a was not changed by Wy-14643 treatment, with Lin28b undetectable in the liver (Figures S1A and S1B).

Hepatocyte-specific *let-7b/c2* knockout results in resistance to obesity

To further analyze the physiological roles of hepatic *let-7*, hepatocyte-specific *let-7b/c2* knockout (*let7b/c2*$^{\Delta Hep}$) mice were generated by mating *Alb-Cre* (Yakar et al., 1999) and *let-7b/c2 floxed* (Madison et al., 2013) mouse lines. *Let7b/c2*$^{\Delta Hep}$ mice showed normal development and fertility, with hepatic *let-7b* and *c2* levels decreased by more than 80% (Figures S1C and S1D). Interestingly, *let7b/c2*$^{\Delta Hep}$ mice showed significantly less weight gain under HFD challenge than similarly treated *let7b/c2*$^{+/+}$ mice (Figures 2A and 2B), without changes in food intake (Figure S1E). Hematoxylin and eosin (H&E) staining and oil red O (ORO) staining revealed less lipid accumulation in the livers of HFD-fed *let7b/c2*$^{\Delta Hep}$ mice than that in similarly treated wild-type mice (Figure 2C). After 8 weeks of HFD feeding, the lean-to-body weight ratio was significantly increased in *let7b/c2*$^{\Delta Hep}$ mice (Figure 2D), whereas both fat-body weight ratios and liver-body weight ratios were significantly lower (Figures 2E and 2F). Serum triglyceride (TG) and total cholesterol (TC) were also markedly decreased in *let7b/c2*$^{\Delta Hep}$ mice (Figures 2G and S1F). These data indicated that *let7b/c2*$^{\Delta Hep}$ mice are resistant to HFD-induced obesity.

In addition, serum alanine aminotransferase (ALT) was decreased in *let7b/c2*$^{\Delta Hep}$ mice, suggesting less hepatotoxicity from HFD feeding (Figure S1G). Although both hepatic TG and TC were significantly decreased (Figures S1H and S1I), non-esterified fatty acids (NEFAs) were increased in *let7b/c2*$^{\Delta Hep}$ mice (Figure S1J). These data suggested that *let7b/c2*$^{\Delta Hep}$ mice had lower constitutive hepatic fatty acid esterification and/or lipid synthesis, whereas fatty acid intake was not changed by the loss of hepatic *let-7b/c2*. In normal chow-diet-fed mice, no significant differences were found in body weight, serum TG, or hepatic TC and TG (Figures S2A, S2B, S2D, and S2E) between the two genotypes, whereas serum TC was slighty decreased in *let7b/c2*$^{\Delta Hep}$ mice (Figures S2C). Previous studies showed that whole-body *let-7* miRNA inhibition modulated glucose metabolism (Frost and Olson, 2011; Zhu et al., 2011). To determine whether these phenotypes were derived from glucose metabolism, insulin, glucose, and pyruvate tolerance tests (ITT, GTT, and PTT, respectively) were performed and no significant differences were found between *let7b/c2*$^{+/+}$ and *let7b/c2*$^{\Delta Hep}$ mice (Figures S2F, S2G, and S2H). These data suggest that hepatic *let7b/c2* disruption improves fatty liver and attenuates obesity during HFD feeding, whereas hepatocyte *let7b/c2* disruption does not affect insulin sensitivity.

Hepatocyte-specific Let-7 sponge expression results in resistance to obesity

miRNA sponges are a well-recognized method to perform loss-of-function analyses of miRNAs *in vivo* and *in vitro* (Ebert and Sharp, 2010). Sponge RNA has complementary binding sites for a given miRNA and is degraded instead of the target mRNAs as a decoy, repressing miRNA activity. To further analyze the role of hepatic *let*-7 in obesity and hepatic

steatosis, an adeno-associated virus 8 (AAV8) designated for hepatocyte-specific expression of let-7 sponge was constructed (let-7 sponge) (Figures S3A and S3B). Primary hepatocytes were transduced with AAV-EGFP, and 5 days after infection, a pronounced EGFP expression was observed, indicating successful infection of cells by AAV. Conversely, let-7 sponge AAV-infected hepatocytes exhibited very low EGFP fluorescence, suggesting that *let-7* miRNA was abundantly expressed in hepatocytes (Figure 2H). EGFP DNA quantification confirmed that the infection efficiency of let-7 sponge expressing AAV was equivalent with AAV-EGFP control (Figure S3C). To inhibit *let-7* activity *in vivo*, the recombinant AAV vectors were intravenously injected to wild-type mice followed by HFD feeding for 8 weeks. Let-7 sponge AAV-injected mice showed less body weight gains starting from 3 weeks after HFD feeding than the EGFP AAV group (Figure 2I). Lipid accumulation was decreased in let-7 sponge AAV-treated liver (Figure S3D). The let-7 sponge group did not show significant differences in lean body weight ratio and liver-body weight ratio (Figures 2J and 2L), whereas the fat-weight-to-body-weight ratio was decreased (Figure 2K). Serum and hepatic TG were also significantly decreased (Figures 2M and S3F), whereas serum TC, hepatic TC, and NEFA did not show significant alterations (Figures S3E, S3G, and S3H). ITT and GTT did not show significant differences (Figures S3I and S3J). Consistent with the phenotype observed in *let7b/c2*$^{\Delta Hep}$ mice, these data indicated that inhibition of mature *let-7* activity resulted in lipid synthesis reduction and obesity resistance.

PPARα target gene mRNAs are lower in *let7b/c2*$^{\Delta Hep}$ livers

To identify potential mechanisms contributing to the observed phenotypes mediated by hepatic *let-7* deletion, RNA sequencing (RNA-seq) was carried out to analyze the gene expression profiles in livers of *let-7b/c2*$^{+/+}$ and *let-7b/c2*$^{\Delta Hep}$ mice fed a HFD. Pathway analysis revealed that PPARα, β/δ, γ, and farnesoid X receptor (FXR) pathways were robustly inhibited in the *let7b/c2*$^{\Delta Hep}$ livers (Figures 3A and S1K; Table S2). These are all ligand-activated nuclear receptors that heterodimerize with RXRα. mRNA-encoding proteins involved in fatty acid oxidation, cell proliferation (Figure 3B), lipid accumulation, and glucose metabolism (Figure 3C) were all found to be decreased by hepatic *let*-7 depletion. Western blot analysis revealed a significant decrease in expression of PPARα target gene protein products, including cytochrome P450 ω-hydroxylase 4A (CYP4A); enoyl-CoA hydratase and 3-hydroxyacyl CoA dehydrogenase (EHHADH); hydroxyacyl-CoA dehydrogenase/3-ketoacyl-CoA thiolase/enoyl-CoA hydratase, α subunit (HADHA); and keratin, type I cytoskeletal 23 (KRT23) in *let7b/c2*$^{\Delta Hep}$ livers (Figure 3D). Several PPARα target genes were repressed even in 1-week HFD-fed livers when the body weight was not altered between *let7b/c2*$^{+/+}$ and *let7b/c2*$^{\Delta Hep}$ mice (Figure S2I), indicating the inhibition of PPAR signaling was independent of body weight change.

RXRα protein is reduced by *Let-7* miRNA inhibition

Nuclear receptors, including the PPAR family and FXR, form obligate heterodimers with RXRα and modulate transcription by binding to their respective responsive elements in the enhancer/promoter regions of target genes (Rigano et al., 2017). Given that PPARα, β/δ, γ, and FXR pathways were significantly repressed, it is reasonable to speculate whether their common heterodimer RXR is regulated by *let*-7. No significant differences in *Rxra* or *Ppara* mRNA levels were found between *let7b/c2*$^{+/+}$ and *let7b/c2*$^{\Delta Hep}$ livers

(Figures S4A and S4B), whereas the RXRα protein in *let-7b/c2*$^{\Delta Hep}$ livers was significantly decreased compared with *let7b/c2*$^{+/+}$ livers (Figure 3F). Then, freshly isolated *let7b/c2*$^{+/+}$ and *let7b/c2*$^{\Delta Hep}$ primary hepatocytes were subjected to RNA and protein analyses, revealing that the RXRα protein but not the *Rxra* mRNA was decreased in *let7b/c2*$^{\Delta Hep}$ hepatocytes (Figures 3E and S4C). Consistently, forced expression of let-7 sponge resulted in a decrease in the RXRα protein but not *Rxra* mRNA (Figures 3G and S4D). In contrast, *let-7c-1* overexpression by AAV led to a significant increase of the RXRα protein but not *Rxra* mRNA (Figures 3H and S4D). A previous study revealed that RXRα inhibition resulted in obesity and amelioration of hepatic steatosis (Yamauchi et al., 2001). An RXRα inhibition experiment was performed in primary hepatocytes by use of the RXRα inhibitor HX-531. Lipid accumulation induced by palmitic acid treatment was repressed by HX-531 administration in hepatocytes (Figure S4E). Western blot analysis of RXRα in the livers of mice fed on chow or HFD and treated with vehicle or Wy-14643 demonstrated that PPARα activation resulted in lower RXRα protein levels under both chow diet and HFD (Figure S4F). These results indicate that *let-7* positively modulates the RXRα protein but not *Rxra* mRNA levels, which may contribute to less hepatic lipid accumulation in livers of *let-7*-deficient mice.

Rnf8 mRNA is a *let-7* miRNA direct target

The ubiquitin-proteasome system is a multi-step process that regulates protein stability and involves enzymes of three different classes. Ubiquitin is activated by the E1 enzyme, and then the E2 enzyme transfers ubiquitin to lysine residues in the target protein. The E3 enzyme binds with the target protein and mediates ubiquitin binding. The polyubiquitinated proteins are then degraded by the 26S proteasome (Glickman and Ciechanover, 2002). Recent studies demonstrated that *Rnf8* encoded an E3 ubiquitin ligase targeting various proteins (Fritsch et al., 2014; Lee et al., 2016; Paul and Wang, 2017). Previous research revealed that RNF8 bound to RXRα in the nucleus (Takano et al., 2004). Because *let7b/c2*$^{\Delta Hep}$ mice exhibited a decrease in the RXRα protein but not *Rxra* mRNA, the question arises whether the RXRα protein is degraded by the ubiquitin-proteasome system. To determine whether *Rnf8* is a direct target of *let*-7 miRNA, the sequence of *Rnf8* was subjected to bioinformatic analysis using open-source algorithms including miRWalk, TargetScan, and microRNA.org. These analyses identified two potential *let-7* miRNA binding sites; site 1 is located within the coding sequence, and site 2 is in the 3′ UTR (Figure 4A). Western blot analyses for the RNF8 protein were performed with an antibody verified with *Rnf8*-overexpressed cell lysates (Figure S4J). Western blot and qRT-PCR analyses revealed that the RNF8 protein and *Rnf8* mRNA were significantly increased in *let7b/c2*$^{\Delta Hep}$ livers respectively (Figures 4B and 4C). The protein and mRNA abundance in mice infected with let-7 sponge-expressed AAV were also significantly elevated (Figures 4D and 4E). In contrast, *pre-let-7c-1*-expressing mouse livers showed a significant decrease of the RNF8 protein (Figure 4F). The *Rnf8* mRNA showed a similar tendency without statistical significance (Figure S4G), suggesting that translational inhibition by *let-7* miRNA contributed to the RNF8 protein decrease more than mRNA decay. To assess whether *Rnf8* mRNA is a direct target of *let-7* miRNA, 3′ UTR reporter assays were performed. The wild-type *Rnf8* 3′ UTR including a predicted *let-7* binding site was cloned into a luciferase reporter vector, and a mutant vector lacking a *let-7* binding site candidate was also

constructed. Using wild-type *Rnf8* 3′ UTR, luciferase activity was significantly decreased by co-transfection with a *let-7c* mimic in HepG2 cells. Conversely, luciferase activity was unchanged with the mutated vector (Figure 4G). These data indicated that *Rnf8* mRNA was a direct target of *let-7* miRNA.

RNF*8* is a E3 ubiquitin ligase for the RXRα protein

To analyze whether RNF8 is involved in RXRα ubiquitination in hepatic cells, RNF8 and RXRα expression vectors were co-transfected into Hepa-1c1c7 (Hepa-1) cells. The cell lysates were subjected to western blot analysis, revealing that the RXRα protein was significantly decreased when RNF8 was co-transfected (Figures 4H and 4I). *Rnf8* mRNA was increased by more than 4,000-fold compared with the control expression vector-transfected group (Figure 4J). Co-transfection with *Rnf8* had no impact on increases in *Rxra* mRNA (Figure 4K). These results suggested that RNF8 expression did not affect *Rxra* mRNA levels but decreased RXRα protein levels *in vitro*.

To determine whether the decrease of the RXRα protein was caused by the ubiquitin-proteasome pathway, Hepa-1 cells transfected with RNF8 and RXRα expression vectors were treated with the proteasome inhibitor MG-132. The MG-132-treated group showed a 1.4-fold increase of the RXRα protein, whereas only a small increase was noted without RNF8 (Figures 4L and S4H). Given that RNF8 is a E3 ubiquitin ligase for RXRα, the RXRα protein should be polyubiquitinated in Hepa-1 cells. Hepa-1 cells transfected with an RXRα expression vector together with or without an RNF8 expression vector were subjected to co-immunoprecipitation (coIP) assays to detect polyubiquitinated RXRα. Western blot analysis of the immunoprecipitated samples revealed that cells transfected with RXRα and RNF8 expression vectors contained significantly more polyubiquitinated RXRα than the non-RNF8 expressing cells (Figure 4M). K48 polyubiquitin is a polyubiquitin chain contributing to protein degradation in the ubiquitin/proteasome pathway. Western blot analysis for RNF8- and RXRα-overexpressed cell lysate was performed with a K48 polyubiquitin-specific antibody, revealing that RNF8 accelerated K48 polyubiquitination of RXRα (Figure S4I). Together with data in the current study, a 3-step inhibition mechanism for the PPARα/RXRα pathway in fatty liver was elucidated (Figure 4N)

DISCUSSION

Although whole-body *let-7* inhibition in transgenic mice expressing *Lin28a* or *Lin28b* improves hepatic steatosis and obesity (Zhu et al., 2011), and a global *let-7* inhibitor partially improves glucose metabolism (Frost and Olson, 2011), the role of *let-7* in hepatic lipid metabolism has previously not been explored. In the current study, for the first time, a pronounced resistance to HFD-induced obesity was noted in mice lacking hepatic *let-7* or in mice infected with AAV expressing a let-7 miRNA sponge. However, *let-7* did not influence insulin sensitivity or glucose tolerance. Mechanistically, a let-7-RNF8-RXRα axis was identified to explain the observed phenotypes in the current study. These results provide novel insights into let-7 miRNA modulation of metabolic diseases.

A striking finding of this study is that the let-7-RNF8-RXRα axis modulates lipid homeostasis during obesity. When hepatic *let-7b/c2* was genetically disrupted or inhibited

by let-7 sponge, the mice showed resistance to HFD-induced fatty liver and obesity. RNA-seq data revealed a consistent downregulation of the target genes of several nuclear receptors, including PPARα, that all shared RXRα as the heterodimer partner, leading to the hypothesis that RXRα is modulated by *let-7* deficiency. Hepatic RXRα protein, but not mRNA, was decreased in the liver of hepatic *let-7*-deficient mice as well as in primary hepatocytes isolated from hepatic *let-7*-deficient mice, possibly contributing to repression of nuclear receptor pathways including PPARα signaling. The positive regulation of *let-7* in RXRα protein expression was further supported by the gain-of-function data from overexpressing *let-7* in both livers and cultured hepatocytes. Given that the RXRα protein, but not mRNA, levels were modulated by *let-7*, a posttranslational modulation of RXRα by *let-7* was suspected. Although RNF8 is known to bind with RXRα in the nucleus (Takano et al., 2004), we found that RNF8 acted as an E3 ubiquitin ligase for RXRα protein in *vitro* and regulated protein degradation of RXRα at the posttranslational level. To explain how RNF8 was increased in hepatic *let-7*-deficient livers, RNF8 protein levels were first found to be decreased in the hepatic *let-7*-deficient livers and increased in hepatic *let-7*-overexpressing livers, and then *Rnf8* mRNA was further identified as a mRNA target of *let-7*. These data together support the existence of a let-7-RNF8-RXRα axis in the liver.

Implicit in the present findings is that decreased RXRα expression may contribute to the phenotype of hepatic *let-7*-deficient mice. Although RXRα inhibition is already known to ameliorate obesity and hepatic steatosis in mice *in vivo* (Yamauchi et al., 2001), we further demonstrated that RXRα inhibition markedly inhibited lipid accumulation in mouse primary hepatocytes in the current study, which together support the view that RXRα inhibition contributes to the improvement of hepatic steatosis and obesity. RXRα is a versatile nuclear receptor contributing to several cellular processes ranging from cell proliferation to lipid metabolism by modulating different target genes (Evans and Mangelsdorf, 2014; Lefebvre et al., 2010). Activation of different RXR-partnered nuclear receptors yields different, or even opposite, effects in modulating the obesity-associated metabolic diseases (Cariou et al., 2006; Gao et al., 2009; Ma et al., 2013; Spruiell et al., 2014). Because hepatic *let*-7 deficiency alleviated fatty liver and obesity in HFD-fed mice, the beneficial effects of RXRα inhibition might be superior to its harmful effects in restricting hepatic lipid accumulation. In this case, the decreased RXRα expression in hepatic *let-7*-deficient mice may contribute to the resistance to HFD-induced obesity and fatty liver. Although decreased RXRα expression by hepatic *let-7* deficiency is suggested to contribute to the phenotype, we cannot rule out the possibility that hepatic *let-7* deficiency improved obesity and fatty liver by other mechanisms.

A PPARα-let-7-RNF8-RXRα negative feedback loop is suggested as one potential downstream pathway after PPARα activation. In the current study, hepatocyte-specific *Ppara* knockout mice in combination with both chemical PPARα agonist and fasting-induced increase of endogenous PPARα ligands were used and confirmed a hepatocyte PPARα-dependent modulation of hepatic *let-7* expression. Once hepatocyte PPARα was activated, expression of the hepatic *let-7* family was inhibited, and the hepatic PPARα signaling pathway was reduced by the proposed let-7-RNF8-RXRα axis once hepatic *let-7* was inhibited, as revealed by using hepatic *let-7*-deficient mice. These results suggest a

possible PPARα-let-7-RNF8-RXRα negative feedback loop, with the detailed mechanisms underlying PPARα-activation-repressed *let-7* expression still awaiting further study.

STAR★METHODS

RESOURCE AVAILABILITY

Lead contact—Further information and requests for resources and reagents should be directed to and will be fulfilled by the Lead Contact, Frank J. Gonzalez (gonzalef@mail.nih.gov).

Materials availability—Plasmids generated in this study are available from the lead contact without restriction.

Data and code availability—RNA-seq data in this study have been deposited at GEO and publicly available as of the date of publication. Accession number is listed in the Key resources table. Other raw data reported in this paper will be shared by the lead contact upon request.

This paper does not report original code.

Any additional information required to reanalyze the data reported in this paper is available from the lead contact upon request.

EXPERIMENTAL MODEL AND SUBJECT DETAILS

Animals—All mouse studies were approved by the NCI Animal Care and Use Committee and performed in accordance with the Institute of Laboratory Animal Resources guidelines. Six-week-old male C57BL/6N mice were purchased from Charles River Laboratories. The *Ppara* wild-type (*Ppara*$^{+/+}$) and hepatocyte-specific *Ppara* knockout (*Ppara*$^{\Delta Hep}$) mice used in this study were described previously (Brocker et al., 2017). Hepatocyte-specific *let-7b/c2* knockout (*let7b/c2*$^{\Delta Hep}$) were generated by mating *Alb-Cre* (Yakar et al., 1999) and *let7-b/c2 flox* (Madison et al., 2013) mouse lines. Mice were housed in a temperature (22°C) and light-controlled vivarium with free access to water and standard rodent chow food, 60% high fat diet (HFD) (S3282 from Bio-Serv) or 0.1% Wy-14,643 diet (F3254 from Bio-Serv). For gavage injection, Wy-14,643 was dissolved in 1% carboxymethyl cellulose and administered at 50 mg/kg. Mouse body composition was analyzed by MRI and Echo Medical Systems in Mouse Metabolism Core in NIDDK. All experiments were started with 7- to 8-week-old male mice.

METHOD DETAILS

Quantitative RT-PCR—Total RNA was extracted from frozen tissues using TRIzol reagent (Themo Fisher Scientific) according to the manufacturer's instructions. The purity and concentration of the total RNA were determined by a NanoDrop spectrophotometer (Thermo Fisher Scientific). One μg of total RNA was reverse transcribed using qScript cDNA synthesis kit (Quantabio). For *let-7* precursor measurement, the total RNA was treated with DNase I (Thermo Fisher scientific) before reverse transcription. Primers for *let-7* miRNA precursors were designed at the stem portion of the hairpin structure as

a previous study (Schmittgen et al., 2008). PerfeCTa SYBR Green Supermix (Quanta Bio) was used for SYBR green detection. For mature *let-7*, the total RNA was reverse-transcribed by Taqman miRNA assay (Thermo Fisher Scientific) and subjected to qRT-PCR as the manufacturer's instructions. *Actb* and *U6* snRNA were used as reference genes for mRNA and miRNA respectively. Polymerase reaction and the fluorescence detection were performed by QuantStudio 7 Flex real-time PCR system (Thermo Fisher Scientific).

Hematoxylin and eosin and oil red O staining—Freshly isolated liver tissues were embedded in OCT compound (Sakura Finetek), and rapidly frozen by liquid nitrogen. The samples were sliced and stained by Histoserve, Inc. Imaging was performed using a KEYENCE BZ-X710 microscope (Keyence).

For primary hepatocytes, 4% paraformaldehyde (Fujifilm wako chemicals), 60% oil red O solution (Muto pure chemicals) and hematoxylin (Muto pure chemicals) were used for fixation and staining respectively. Morphometric analyses were performed by ImageJ software (NIH).

Biochemical analyses for triglyceride, total cholesterol, and non-esterified fatty acid—Frozen liver tissues were homogenized by Precellys tissue homogenizer (Bertin Instruments) in 50 mM Tris-HCl with 5% Triton X-100 as previously described (Li et al., 2017). The lysate and serum samples were subjected to L-type Triglyceride M (Fujifilm Wako Diagnostics), Cholesterol E (Fujifilm Wako Diagnostics), and HR series NEFA-HR(2) (Fujifilm Wako Diagnostics) for measuring triglyceride (TG), total cholesterol (TC), and non-esterified fatty acid concentrations (NEFA), respectively.

Biochemical analysis for serum alanine aminotransferase—Serum samples were subjected to commercial ALT assay kit (Catachem) and monitored at 340 nm for 10 min with a microplate reader (BioAssay Systems).

Insulin, Glucose, and Pyruvate tolerance test—Intraperitoneal insulin, glucose, and pyruvate tolerance test was performed with the protocol provided from National Mouse Metabolic Phenotyping Center. One drop blood was taken via tail tip cut from 4 h-fasted mice. The blood glucose was measured by glucometer for a baseline. Then, 0.5 U/mL Humalin R (Eli Lilly), 20% Dextrose (Hospira) and sodium pyruvate (Sigma) was intraperitoneally injected to the mice at 0.5 U/kg, 1g/kg and 1g/kg, respectively. Blood glucose was measured at 15, 30, 45, 60, and 120 min after injection.

Construction of hepatocyte-specific let-7 sponge and pre-let-7c-1 expression adeno-associated virus (AAV) vector—The albumin promoter-driven self-complementary EGFP-AAV plasmid (pscAAV-ALBp-EGFP) described in a previous study (Kim et al., 2019) was used as a backbone vector. Single strand let-7 sponge and the complementary oligos shown in Figure S3A were purchased from Integrated DNA Technologies. The oligos were annealed and cloned into pscAAV-ALBp-EGFP plasmid with *Not I* and *Stu I* restriction enzymes. For *pre-let-7c-1* expression AAV, the 470 bp mouse genomic sequence around *pre-let-7c-1* was amplified using custom primers (Table S3) from a MirLet7c-1 expression plasmid (Origene). The amplified fragments were cloned

into pscAAV-ALBp-EGFP plasmid with *Not I, Stu I,* and *EcoR V* restriction enzymes. The plasmids were transfected into HEK293T cells to produce AAV8 vectors by the triple transfection method then purified using polyethylene glycol precipitation followed by cesium chloride density gradient fractionation as previously described (Park et al., 2009). AAV was transduced into primary hepatocyte at 1×10^5 infectious unit (ifu) and one mouse at 1×10^{11} ifu via tail vein injection respectively. For validation of infection efficiency, EGFP DNA isolated from the primary hepatocytes by QIAamp DNA Mini Kit (QIAGEN) and concentrated AAV solutions were amplified by qRT-PCR, and then analyzed by comparative Ct method.

Primary hepatocyte isolation and culture—Primary hepatocytes from C57BL/6N mice were isolated by a two-step perfusion method modified from a previous study (Yagai et al., 2014). Hank's balanced salt solution (HBSS) without $CaCl_2$, $MgCl_2$ and $MgSO_4$ (Thermo Fisher Scientific) was used as basic solution. 25 mL HBSS with 1mM EDTA was perfused into liver via the portal vein for one mouse. Then, 25 mL HBSS containing 0.025% collagenase type I (Thermo Fisher Scientific), 0.025% collagenase type II (Thermo Fisher Scientific), 0.005% trypsin inhibitor (Thermo Fisher Scientific) and 0.075% $CaCl_2$:H_2O (Mallinckrodt Pharmaceuticals) was perfused. The digested liver was passed through a 70-μm cell strainer. Hepatocytes were precipitated by centrifugation at 50 × g for 2 min. The dead hepatocytes were removed by Percoll (GE Healthcare) density centrifugation at 70 × g for 10 min. Hepatocytes were cultured in collagen-coated plates (Corning) with William's Medium E (Lonza) containing 400 ng/ml dexamethasone (Sigma-Aldrich), 1 x insulin-transferrin-selenium (Sigma-Aldrich), 1 x Glutamax (Thermo Fisher Scientific), 25 mM HEPES (Thermo Fisher Scientific), and 5% FBS (Gemini).

RNA-seq and pathway analysis—Total liver RNA was prepared by RNeasy plus mini kit (QIAGEN). The purity and concentration of extracted RNA were measured by 4200 TapeStation system (Agilent). Library prep followed by RNA-sequencing were performed by the National Cancer Institute Sequencing Facility. RNA-seq library was prepared by TruSeq Stranded mRNA Library Prep (Illumina). The library was analyzed by HiSeq3000/4000 system (Illumina) with paired-end 150 read length. The RNA-seq datasets generated during this study are available at Gene Expression Omnibus (Accession number: GSE165521). The comprehensive gene expression profile was subjected to Ingenuity Pathway Analysis (QIAGEN).

Ubiquitination assay for RXRα protein—pSG5-mouse *Rxra* (Leid et al., 1992) and pCMV6-mouse *Rnf8* (Origene) expression plasmids were co-transfected into Hepa-1c1c7 cells (ATCC) using Lipofectamine 3000 (Thermo Fisher Scientific). pRK5-HA-Ubiquitin-WT (Addgene) were co-transfected for polyubiquitin type analysis. Three days after transfection, cell lysates were harvested with RIPA buffer. For ubiquitination assays, 20 μM MG-132 (Sigma-Aldrich) was added to the medium and the cells were cultured for 4 h before harvesting. For RXRα immunoprecipitation, rabbit monoclonal RXRα antibody (Abcam) was added to 400 μL cell lysate adjusted at 1 mg/ml protein concentration. The cell lysate was incubated at 4°C for overnight. The following day, protein A agarose (Sigma-Aldrich) was added and incubated for 2 h at 4°C. Then, the RXRα-ubiquitin complexes

were added to Laemmli sample buffer (Bio-Rad) with 5% 2-mercaptoethanol and heated to 95°C for 5 min. The samples were subsequently analyzed by western blot.

Western blot analysis—Liver tissue or cell samples were lysed in RIPA buffer. 10 μg protein was added to Laemmli sample buffer (Bio-Rad) with 5% 2-mercaptoethanol at 95°C for 5 min. The samples were loaded in Criterion TGX precast gel (Bio-Rad), separated by electrophoresis, then transferred using a Trans-Blot Turbo Transfer System (Bio-Rad). The protein transferred PVDF membrane was incubated with 5% skim milk containing primary antibody overnight at 4°C. Horseradish peroxidase-conjugated secondary antibodies in 5% skim milk was incubated for two h at room temperature. After the incubation, the washed membrane was exposed to SuperSignal West Dura Extended Duration Substrate (Thermo Fisher Scientific) for luminol reaction. Chemiluminescence was imaged and quantified using a ChemiDoc MP Imaging System (Bio-Rad). Anti-RXRα (Abcam, ab125001) and anti-PPARα (Abcam, ab126285) antibodies were used for the protein detection.

Dual luciferase reporter assay—*Let-7adf* cluster EP fragments were amplified from mouse genome by the primers listed in Table S3. The insert was digested and cloned into pGL4.27 (Promega). The constructed reporter vector and phRL-TK renilla luciferase expression vector (Promega) were co-transfected into primary hepatocyte by Lipofectamine 3000 (Thermo Fisher Scientific). Three days later, the cells were lysed using the passive lysis buffer supplied in Firefly & Renilla Luciferase Single Tube Assay Kit (Biotium). Dual luciferase assay was performed as the manufacture's protocol and Veritas Microplate Luminometer (Turner BioSystems). For the mouse *Rnf8* 3′UTR reporter assay, *Rnf8* 3′UTR wild-type (WT) and mutant (Mut) fragments in Table S1 were purchased from Integrated DNA Technologies. The UTR inserts were cloned into pmirGLO vector (Promega) for *Rnf8* 3′UTR WT and Mut reporters, respectively. 20 nM *let-7c* mimic or the scramble control (Dharmacon) was transfected into HepG2 cells by Lipofectamine 3000 (Thermo Fisher Scientific). The next day, reporter vectors were transfected using the same technique. Five days later, the cells were lysed and subjected to dual luciferase assay as same manner above.

QUANTIFICATION AND STATISTICAL ANALYSIS

Statistical analysis and graphing of the data were performed using GraphPad Prism. Data are presented as mean ± SE for biological replicates. Statistical significance is indicated by the following annotations: *$p < 0.05$, $^{\#}p < 0.01$, $^{\S}p < 0.001$ in Figures 1A and 1C and *$p < 0.05$, **$p < 0.01$, ***$p < 0.001$ in other Figures. p values were calculated by two-sided paired t tests followed by Bonferroni analysis. Please note that statistical details are found in the figure legends.

Supplementary Material

Refer to Web version on PubMed Central for supplementary material.

ACKNOWLEDGMENTS

We thank Linda G. Byrd for assistance with the mouse studies and Oksana Gavrilova for mouse body composition analysis. This work was funded by the National Cancer Institute Intramural Research Program. T. Yagai and S. Takahashi were supported in part by a fellowship from the Japan Society for the Promotion of Science. The funding

sponsors had no role in the design, collection, analysis, or interpretation of data; in the writing of the manuscript; or in the decision to submit the manuscript for publication.

REFERENCES

Brocker CN, Yue J, Kim D, Qu A, Bonzo JA, and Gonzalez FJ (2017). Hepatocyte-specific PPARA expression exclusively promotes agonist-induced cell proliferation without influence from nonparenchymal cells. Am. J. Physiol. Gastrointest. Liver Physiol 312, G283–G299. [PubMed: 28082284]

Büssing I, Slack FJ, and Grosshans H (2008). let-7 microRNAs in development, stem cells and cancer. Trends Mol. Med 14, 400–409. [PubMed: 18674967]

Cariou B, van Harmelen K, Duran-Sandoval D, van Dijk TH, Grefhorst A, Abdelkarim M, Caron S, Torpier G, Fruchart J-C, Gonzalez FJ, et al. (2006). The farnesoid X receptor modulates adiposity and peripheral insulin sensitivity in mice. J. Biol. Chem. 281, 11039–11049. [PubMed: 16446356]

Ebert MS, and Sharp PA (2010). MicroRNA sponges: progress and possibilities. RNA 16, 2043–2050. [PubMed: 20855538]

Evans RM, and Mangelsdorf DJ (2014). Nuclear Receptors, RXR, and the Big Bang. Cell 157, 255–266. [PubMed: 24679540]

Fritsch J, Stephan M, Tchikov V, Winoto-Morbach S, Gubkina S, Kabelitz D, and Schütze S (2014). Cell fate decisions regulated by K63 ubiquitination of tumor necrosis factor receptor 1. Mol. Cell. Biol 34, 3214–3228. [PubMed: 24980434]

Frost RJ, and Olson EN (2011). Control of glucose homeostasis and insulin sensitivity by the Let-7 family of microRNAs. Proc. Natl. Acad. Sci. USA 108, 21075–21080. [PubMed: 22160727]

Gao J, He J, Zhai Y, Wada T, and Xie W (2009). The constitutive androstane receptor is an anti-obesity nuclear receptor that improves insulin sensitivity. J. Biol. Chem 284, 25984–25992. [PubMed: 19617349]

Glickman MH, and Ciechanover A (2002). The ubiquitin-proteasome proteolytic pathway: destruction for the sake of construction. Physiol. Rev 82, 373–428. [PubMed: 11917093]

Johnson SM, Grosshans H, Shingara J, Byrom M, Jarvis R, Cheng A, Labourier E, Reinert KL, Brown D, and Slack FJ (2005). RAS is regulated by the let-7 microRNA family. Cell 120, 635–647. [PubMed: 15766527]

Jovanovic M, and Hengartner MO (2006). miRNAs and apoptosis: RNAs to die for. Oncogene 25, 6176–6187. [PubMed: 17028597]

Kersten S, Seydoux J, Peters JM, Gonzalez FJ, Desvergne B, and Wahli W (1999). Peroxisome proliferator-activated receptor α mediates the adaptive response to fasting. J. Clin. Invest 103, 1489–1498. [PubMed: 10359558]

Kim D, Brocker CN, Takahashi S, Yagai T, Kim T, Xie G, Wang H, Qu A, and Gonzalez FJ (2019). Keratin 23 is a peroxisome proliferator-activated receptor α–dependent, MYC-amplified oncogene that promotes hepatocyte proliferation. Hepatology 70, 154–167. [PubMed: 30697791]

Lee HJ, Li CF, Ruan D, Powers S, Thompson PA, Frohman MA, and Chan CH (2016). The DNA damage transducer RNF8 facilitates cancer chemoresistance and progression through Twist activation. Mol. Cell 63, 1021–1033. [PubMed: 27618486]

Lefebvre P, Benomar Y, and Staels B (2010). Retinoid X receptors: common heterodimerization partners with distinct functions. Trends Endocrinol. Metab 21, 676–683. [PubMed: 20674387]

Leid M, Kastner P, Lyons R, Nakshatri H, Saunders M, Zacharewski T, Chen J-Y, Staub A, Garnier J-M, Mader S, et al. (1992). Purification, cloning, and RXR identity of the HeLa cell factor with which RAR or TR heterodimerizes to bind target sequences efficiently. Cell 68, 377–395. [PubMed: 1310259]

Li G, Xie C, Lu S, Nichols RG, Tian Y, Li L, Patel D, Ma Y, Brocker CN, Yan T, et al. (2017). Intermittent fasting promotes white adipose browning and decreases obesity by shaping the gut microbiota. Cell Metab. 26, 672–685.e4. [PubMed: 28918936]

Liu Y, Chen Q, Song Y, Lai L, Wang J, Yu H, Cao X, and Wang Q (2011). MicroRNA-98 negatively regulates IL-10 production and endotoxin tolerance in macrophages after LPS stimulation. FEBS Lett. 585, 1963–1968. [PubMed: 21609717]

Ma Y, Huang Y, Yan L, Gao M, and Liu D (2013). Synthetic FXR agonist GW4064 prevents diet-induced hepatic steatosis and insulin resistance. Pharm. Res 30, 1447–1457. [PubMed: 23371517]

Madison BB, Liu Q, Zhong X, Hahn CM, Lin N, Emmett MJ, Stanger BZ, Lee JS, and Rustgi AK (2013). LIN28B promotes growth and tumorigenesis of the intestinal epithelium via Let-7. Genes Dev. 27, 2233–2245. [PubMed: 24142874]

Mayr C, Hemann MT, and Bartel DP (2007). Disrupting the pairing between let-7 and Hmga2 enhances oncogenic transformation. Science 315, 1576–1579. [PubMed: 17322030]

Park TK, Wu Z, Kjellstrom S, Zeng Y, Bush RA, Sieving PA, and Colosi P (2009). Intravitreal delivery of AAV8 retinoschisin results in cell type-specific gene expression and retinal rescue in the Rs1-KO mouse. Gene Ther. 16, 916–926. [PubMed: 19458650]

Paul A, and Wang B (2017). RNF8- and Ube2S-dependent ubiquitin lysine 11-linkage modification in response to DNA damage. Mol. Cell 66, 458–472.e5. [PubMed: 28525740]

Piskounova E, Viswanathan SR, Janas M, LaPierre RJ, Daley GQ, Sliz P, and Gregory RI (2008). Determinants of microRNA processing inhibition by the developmentally regulated RNA-binding protein Lin28. J. Biol. Chem 283, 21310–21314. [PubMed: 18550544]

Rigano D, Sirignano C, and Taglialatela-Scafati O (2017). The potential of natural products for targeting PPARα. Acta Pharm. Sin. B 7, 427–438. [PubMed: 28752027]

Schickel R, Boyerinas B, Park SM, and Peter ME (2008). MicroRNAs: key players in the immune system, differentiation, tumorigenesis and cell death. Oncogene 27, 5959–5974. [PubMed: 18836476]

Schmittgen TD, Lee EJ, Jiang J, Sarkar A, Yang L, Elton TS, and Chen C (2008). Real-time PCR quantification of precursor and mature microRNA. Methods 44, 31–38. [PubMed: 18158130]

Schulte LN, Eulalio A, Mollenkopf HJ, Reinhardt R, and Vogel J (2011). Analysis of the host microRNA response to Salmonella uncovers the control of major cytokines by the let-7 family. EMBO J. 30, 1977–1989. [PubMed: 21468030]

Shah YM, Morimura K, Yang Q, Tanabe T, Takagi M, and Gonzalez FJ (2007). Peroxisome proliferator-activated receptor α regulates a microRNA-mediated signaling cascade responsible for hepatocellular proliferation. Mol. Cell. Biol 27, 4238–4247. [PubMed: 17438130]

Spruiell K, Richardson RM, Cullen JM, Awumey EM, Gonzalez FJ, and Gyamfi MA (2014). Role of pregnane X receptor in obesity and glucose homeostasis in male mice. J. Biol. Chem 289, 3244–3261. [PubMed: 24362030]

Stefani G, and Slack FJ (2008). Small non-coding RNAs in animal development. Nat. Rev. Mol. Cell Biol 9, 219–230. [PubMed: 18270516]

Takano Y, Adachi S, Okuno M, Muto Y, Yoshioka T, Matsushima-Nishiwaki R, Tsurumi H, Ito K, Friedman SL, Moriwaki H, et al. (2004). The RING finger protein, RNF8, interacts with retinoid X receptor α and enhances its transcription-stimulating activity. J. Biol. Chem 279, 18926–18934. [PubMed: 14981089]

Yagai T, Miyajima A, and Tanaka M (2014). Semaphorin 3E secreted by damaged hepatocytes regulates the sinusoidal regeneration and liver fibrosis during liver regeneration. Am. J. Pathol 184, 2250–2259. [PubMed: 24930441]

Yakar S, Liu JL, Stannard B, Butler A, Accili D, Sauer B, and LeRoith D (1999). Normal growth and development in the absence of hepatic insulin-like growth factor I. Proc. Natl. Acad. Sci. USA 96, 7324–7329. [PubMed: 10377413]

Yamauchi T, Waki H, Kamon J, Murakami K, Motojima K, Komeda K, Miki H, Kubota N, Terauchi Y, Tsuchida A, et al. (2001). Inhibition of RXR and PPARgamma ameliorates diet-induced obesity and type 2 diabetes. J. Clin. Invest. 108, 1001–1013. [PubMed: 11581301]

Zhu H, Shyh-Chang N, Segrè AV, Shinoda G, Shah SP, Einhorn WS, Takeuchi A, Engreitz JM, Hagan JP, Kharas MG, et al.; DIAGRAM Consortium; MAGIC Investigators (2011). The Lin28/let-7 axis regulates glucose metabolism. Cell 147, 81–94. [PubMed: 21962509]

Highlights

- PPARα activation represses let-7 microRNA expression
- let-7 microRNA promotes decay of *Rnf8* mRNA and loss of RNF8 protein
- RNF8 promotes RXRα protein degradation
- let-7-RNF8-RXRα axis controls hepatic lipid metabolism through a negative feedback loop

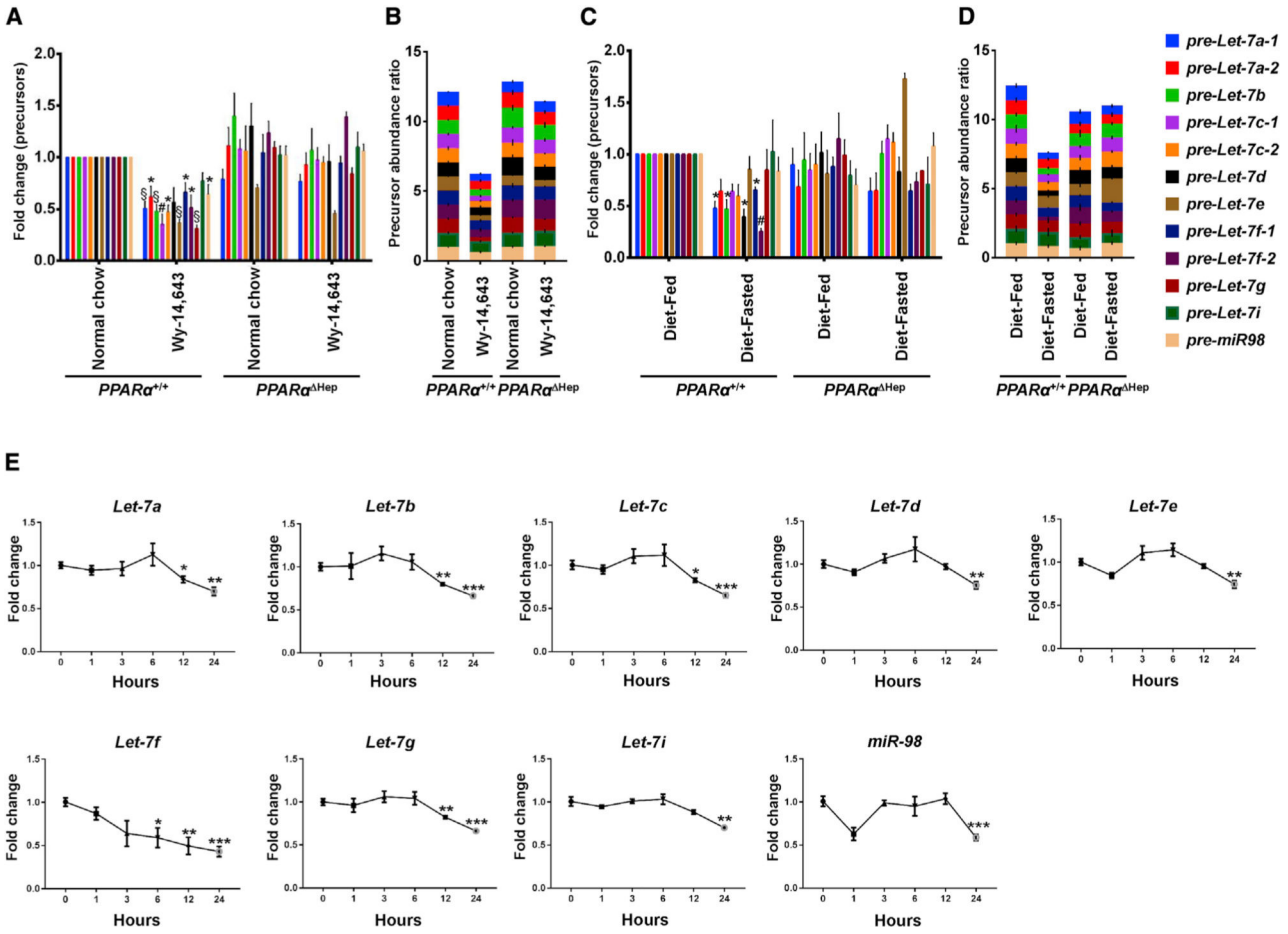

Figure 1. Expression of *let-7* miRNA family members is decreased in mouse liver in response to PPARα activation

(A–D) Fold change of *let-7* miRNA precursors in PPARα-activated *Ppara*$^{+/+}$ and *Ppara*$^{\Delta Hep}$ mouse livers measured by qRT-PCR. Individual *let-7* miRNA precursor expression in livers treated with Wy-14,643 (A) or overnight fasting (C). Precursor abundance ratios in mice treated with Wy-14,643 (B) or overnight fasting (D). Data are normalized to *Actb* expression and presented as mean ± SEM (n = 4 mice per group; *p < 0.05, $^{\#}$p < 0.01, §p < 0.001)

(E) Time course of mature *let-7* miRNA abundance in wild-type mouse liver after Wy-14,643 administration measured by qRT-PCR. Data are normalized to *U6* expression and presented as mean ± SEM (n = 4 mice per group; *p < 0.05, **p < 0.01, ***p < 0.001)

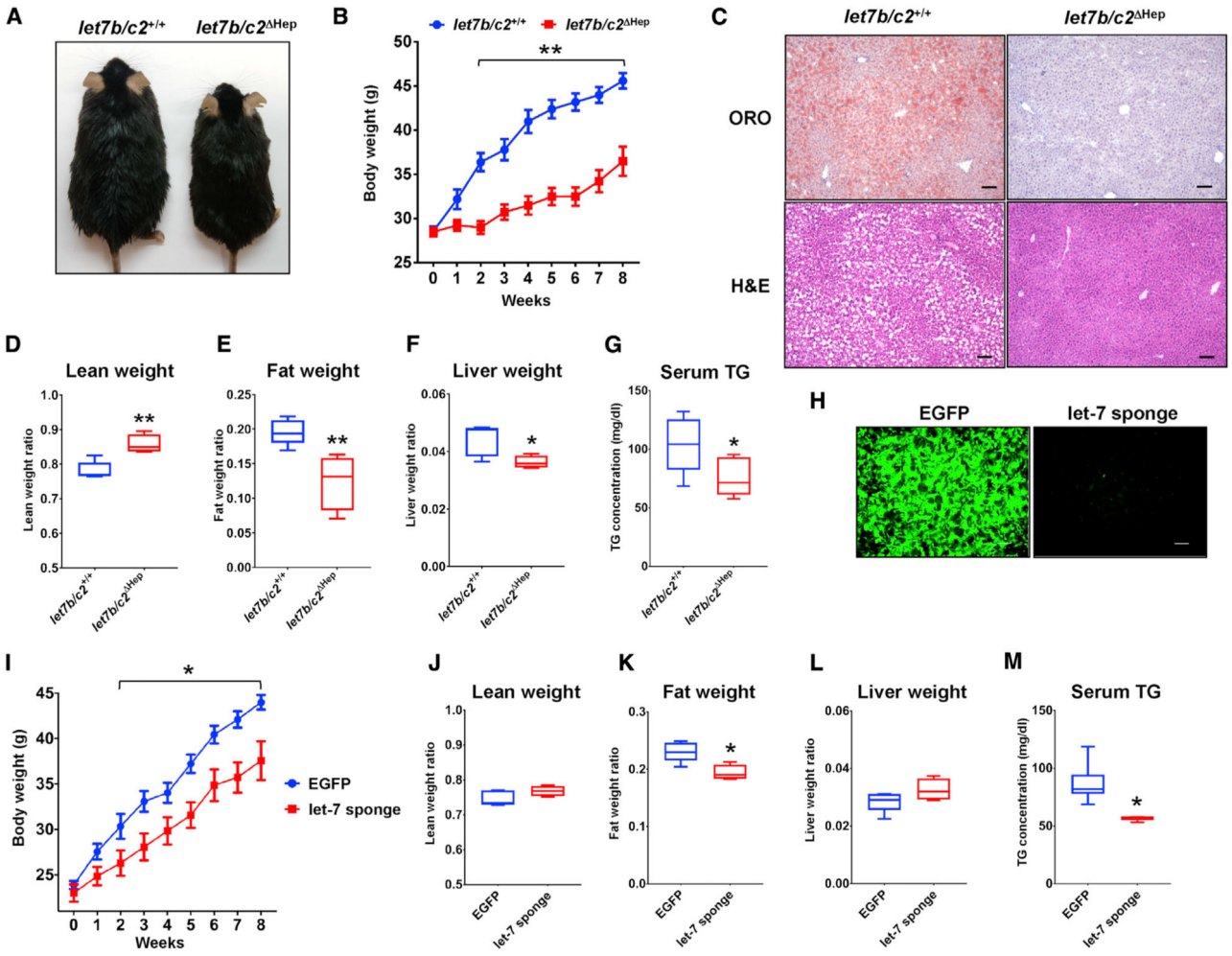

Figure 2. *let7b/c2*$^{\Delta Hep}$ and let-7 sponge AAV-transduced mice are resistant to HFD-induced obesity

(A) *let7b/c2*$^{+/+}$ and *let7b/c2*$^{\Delta Hep}$ mice after HFD feeding for 8 weeks.

(B) Body weight alterations of *let7b/c2*$^{+/+}$ and *let7b/c2*$^{\Delta Hep}$ mice during HFD feeding.

(C) Oil red O and H&E staining of *let7b/c2*$^{+/+}$ and *let7b/c2*$^{\Delta Hep}$ liver sections after HFD feeding. Bars, 100 μM.

(D–F) Tissue weight ratio of lean (D), fat (E), and liver (F) to total body weight for *let7b/c2*$^{+/+}$ and *let7b/c2*$^{\Delta Hep}$ mice after HFD feeding.

(G) Biochemical analysis for serum triglycerides (TGs) in *let7b/c2*$^{+/+}$ and *let7b/c2*$^{\Delta Hep}$ mice after HFD feeding.

(H) EGFP fluorescence in mouse primary hepatocytes infected with either EGFP or let-7 sponge AAV vectors after 5 days in culture. Bars, 300 μm.

(I) Body weight alterations in wild-type mice infected with EGFP or let-7 sponge expressing AAV and then placed on HFD for 8 weeks.

(J–L) Tissue weight ratio of lean (J), fat (K), and liver (L) to total body weight for wild-type mice infected with EGFP or let-7 sponge expressing AAV then placed on HFD for 8 weeks.

(M) Biochemical analyses for serum TG concentration in EGFP and let-7 sponge AAV-infected mice after HFD feeding.

Data are presented as mean ± SEM (n = 4–5 mice per group; *p < 0.05, **p < 0.01)

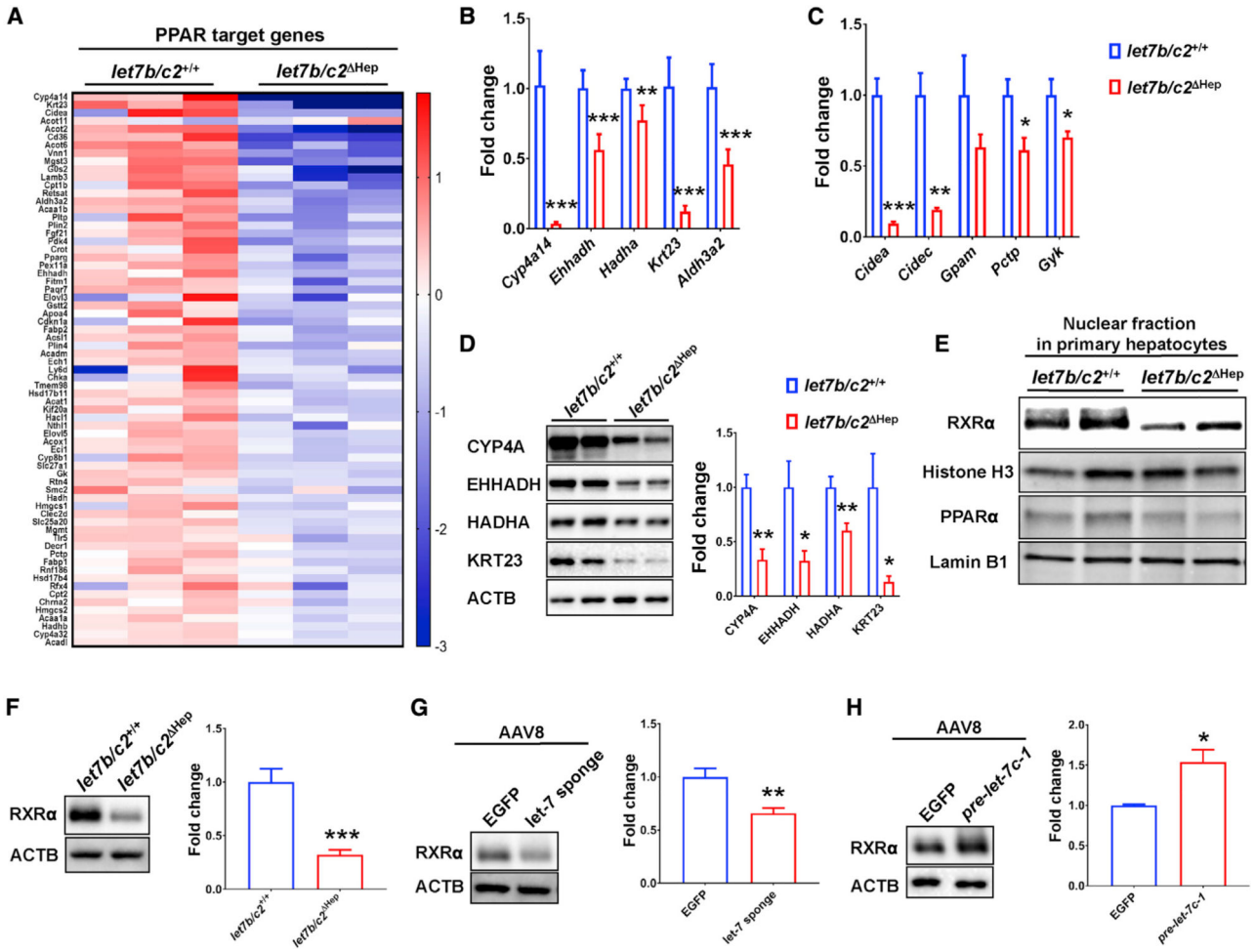

Figure 3. PPARα target gene expressions were repressed by RXRα protein reduction in *let7b/c2*$^{\Delta Hep}$ and let-7 sponge AAV-transduced mice

(A) Heatmap of PPARα target genes identified by differential gene expression analysis of RNA-seq data from *let7b/c2*$^{+/+}$ and *let7b/c2*$^{\Delta Hep}$ livers after HFD feeding.

(B and C) mRNA analysis by qRT-PCR of PPARα target genes involved in fatty acid oxidation and cell proliferation (B) and lipid accumulation and glucose metabolism (C) in HFD-fed *let7b/c2*$^{+/+}$ and *let7b/c2*$^{\Delta Hep}$ livers.

(D) Western blot analysis for PPARα target genes in HFD-fed *let7b/c2*$^{+/+}$ and *let7b/c2*$^{\Delta Hep}$ liver lysates.

(E) Western blot analysis of PPARα and RXRα protein expression in nuclear fractions isolated from *let7b/c2*$^{+/+}$ and *let7b/c2*$^{\Delta Hep}$ hepatocytes.

(F–H) Western blot analysis of RXRα and the densiometric quantification in whole-liver lysates from *let7b/c2*$^{\Delta Hep-}$ mice (F), let-7 sponge expressing AAVinflected mice (G), and *pre-let-7c-1*–AAVinfected mice (H).

Data are presented as mean ± SEM (n = 4–5 mice per group; *p < 0.05, **p < 0.01, ***p < 0.001

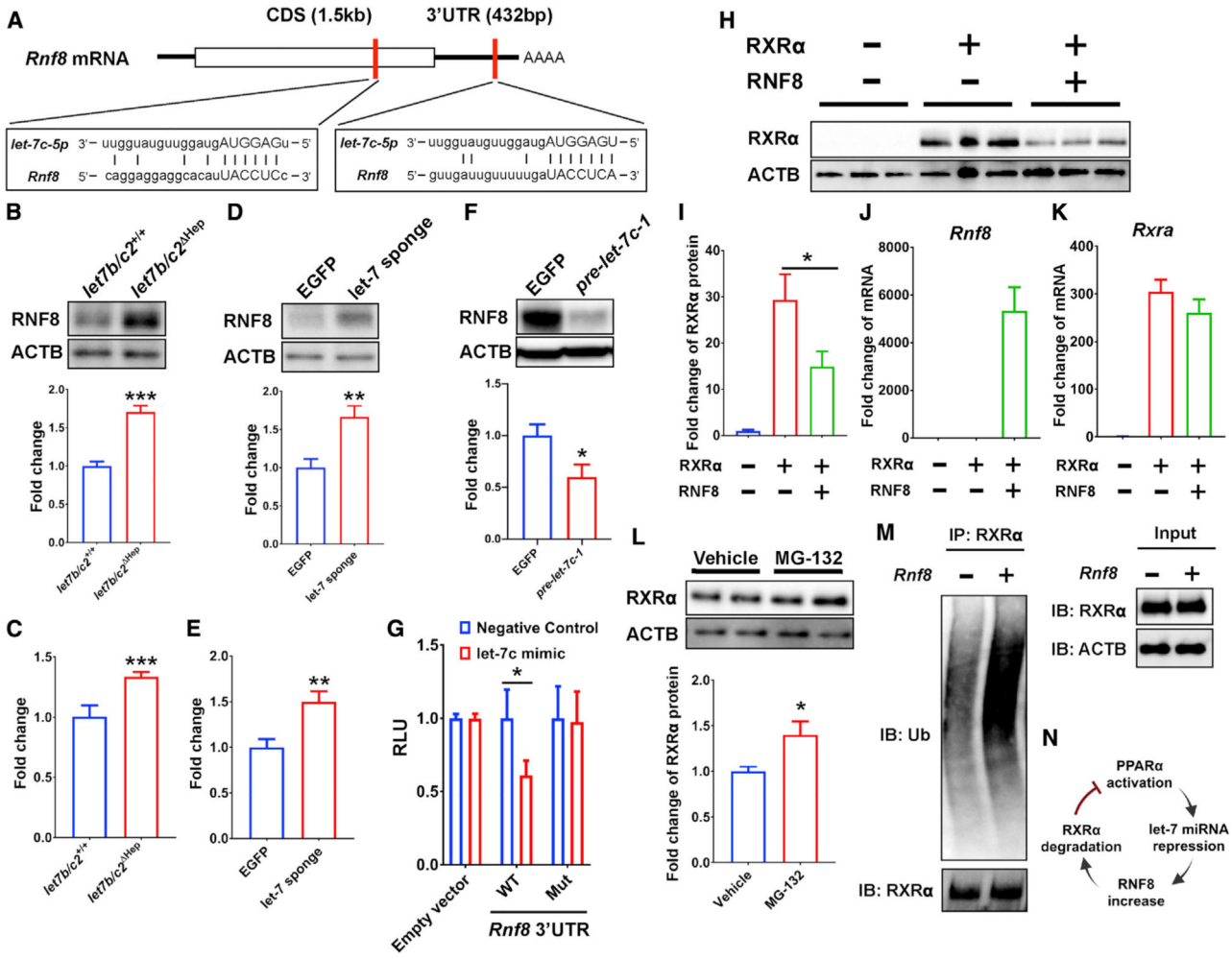

Figure 4. RNF8 is decayed by let-7 miRNA, and RXRα protein is ubiquitinated by RNF8 E3 ubiquitin ligase

(A) Predicted *let-7* miRNA binding sites in *Rnf8* mRNA.

(B–F) Western blot analysis and densitometric quantification of RNF8 protein (B, D, and F) and qRT-PCR of *Rnf8* mRNA (C and E) in *let7b/c2*$^{+/+}$ and *let7b/c2*$^{\Delta Hep}$ (B and C); EGFP and let-7 sponge AAV-transduced (D and E); EGFP and *pre-let-7c-1* AAV-transduced (F) livers treated with HFD feeding.

(G) 3′ UTR reporter assays in HepG2 cells transfected with *Rnf8* wild-type or mutant 3′ UTR reporter constructs and a let-7c mimic expression vector.

(H and I) Western blot analysis (H) and densitometric quantification (I) of RXRα expression in *Rxra*- and *Rnf8*-transfected Hepa-1 cells.

(J and K) Fold change of *Rnf8* (J) and *Rxra* (K) mRNA by qRT-PCR analysis in *Rxra*- and *Rnf8*-transfected Hepa-1 cells.

(L) Western blot analysis and the densitometric quantification of RXRα in *Rxra*- and *Rnf8*-transfected Hepa-1 cells treated with the proteasome inhibitor MG-132.

(M) Ubiquitination assays for *Rxra*- and *Rnf8*-transfected and MG-132-treated Hepa-1 cells. RXRα was immunoprecipitated and polyubiquitin detected by anti-ubiquitin antibody. RXRα expression was confirmed in whole-cell lysate as input.

(N) Scheme of 3-step inhibition for PPARα/RXRα pathway that the current study demonstrates.

KEY RESOURCES TABLE

REAGENT or RESOURCE	SOURCE	IDENTIFIER
Antibodies		
Mouse monoclonal anti-CYP4A	Santa Cruz	Cat# sc-271983; RRID: AB_10715105
Mouse monoclonal anti-RNF8	Santa Cruz	Cat# sc-271462; RRID: AB_10648902
Mouse monoclonal anti-Ub	Santa Cruz	Cat# sc-8017; RRID: AB_628423
Mouse monoclonal HA-probe	Santa Cruz	Cat# sc-7392; RRID: AB_627809
Mouse monoclonal β-Actin	Santa Cruz	Cat# sc-47778; RRID: AB_626632
Rabbit polyclonal anti-EHHADH	Proteintec	Cat# 26570-1-AP; RRID: AB_2880556
Rabbit polyclonal anti-HADHA	Proteintec	Cat# 10758-1-AP; RRID: AB_2115593
Rabbit polyclonal anti-KRT23	Origene	Cat# TA321839
Rabbit monoclonal anti-RXRα	Abcam	Cat# ab125001; RRID: AB_10975632
Rabbit polyclonal anti-Histon H3	Abcam	Cat# ab1791; RRID: AB_302613
Rabbit polyclonal anti-PPARα	Abcam	Cat# ab126285
Rabbit monoclonal anti-K48-linkage Ubiquitin	Cell Signaling Technology	Cat# 8081; RRID: AB_10859893
Bacterial and virus strains		
AAV8-Alb-EGFP; -let-7 sponge; -pre-*let-7c-1*	This paper	N/A
Chemicals, peptides, and recombinant proteins		
Protease inhibitor cocktail	Sigma-Aldrich	Cat# P9599
Protein A Agarose	Sigma-Aldrich	Cat# P2545
Wy-14,643	APExBIO	Cat# A4305
MG-132	Sigma-Aldrich	Cat# M8699
Dexamethasone	Sigma-Aldrich	Cat# D2915
Insulin-Transferrin-Serenium	Sigma-Aldrich	Cat# I3146
Glutamax Supplement	Thermo Fisher Scientific	Cat# 35050079
HEPES	Thermo Fisher Scientific	Cat# 15630080
Humulin R (human recombinant insulin)	Eli Lilly	N/A
Critical commercial assays		
Taqman microRNA Assay	Thermo Fisher Scientific	Cat# 4427975 Assay ID:000377; 000378; 000379; 002283; 002406; 000382; 002282; 002221; 000577
L-Type Triglyceride M	Fujifilm Wako Diagnostics	Cat# 994-02891; 990-02991
Cholesterol E	Fujifilm Wako Diagnostics	Cat# 999-02601
HR Series NEFA-HR(2)	Fujifilm Wako Diagnostics	Cat# 999-34691; 995-34791; 991-34891; 993-35191; 276-76491
SimpleChIP Plus Enzymatic Chromatin IP kit	Cell Signaling Technology	Cat# 9005
ALT assay kit	Catachem Inc	Cat# V165-12
Deposited data		
Raw and analyzed data	This paper	GEO: GSE165521

REAGENT or RESOURCE	SOURCE	IDENTIFIER
Experimental models: Cell lines		
Human: Hep G2 cells	ATCC	Cat# HB-8065
Mouse: Hepa-1c1c7 cells	ATCC	Cat# CRL-2026
Experimental models: Organisms/strains		
Mouse: C57BL/6	Charles River Laboratories	Strain Code: 027
Mouse: *Ppara* wild-type ($Ppara^{+/+}$)	Brocker et al., 2017	N/A
Mouse: Hepatocyte-specific *Ppara* knockout ($Ppara^{\Delta Hep}$)	Brocker et al., 2017	N/A
Mouse: *Alb-Cre*	Yakar et al., 1999	N/A
Mouse: *let7b/c2* flox	Madison et al., 2013	N/A
Oligonucleotides		
miRIDIAN microRNA Mimic Negative Control #1	Dhamacon	Cat# CN-001000-01-05
miRIDIAN microRNA hsa-let-7c-5p mimic	Dhamacon	Cat# C-300477-03-0005
let-7 sponge; see Figure S4	Integrated DNA Technologies	N/A
Primers for qPCR; see Table S1	This paper	N/A
Recombinant DNA		
pscAAV-ALBp-EGFP	Kim et al., 2019	N/A
pSR449B, pAAV8RC	Park et al., 2009	N/A
pCMV-MIR-MirLet7c-1	Origene	Cat# SC400710
pSG5-mouse *Rxra*	Leid et al., 1992	N/A
pCMV6-mouse *Rnf8*	Origene	Cat# MR207821
pRK5-HA-Ubiquitin-WT	Addgene	Cat# 17608
pGL4.27	Promega	Cat# E8451
phRL-TK	Promega	Cat# E6241
pmirGLO	Promega	Cat# E1330
Software and algorithms		
GraphPad Prism 7.0	https://www.graphpad.com:443/	N/A
Ingenuity Pathway Analysis	https://digitalinsights.qiagen.com/products-overview/discovery-insights-portfolio/content-exploration-and-databases/qiagen-ipa/	N/A